Model predictive control of viral amplification process: numerical and experimental investigation

Laurent Dewasme[1], Guillaume Jeanne[2], Lydia Saint Cristau[2],
Alain Vande Wouwer[1]

***Abstract*—Based on an available digital twin of a Vero cell culture process composed of a dynamic mechanistic model and a soft sensor, the impact of viral amplification is studied and optimized in the process development environment of Sanofi (Marcy l'Etoile, France). The soft sensor (an extended Kalman filter) uses Raman probe online measurements of biomass and some metabolites to estimate the infection titer and is combined with a model predictive controller that aims to optimize the infection titer while regulating the main substrate concentration level. The setup is validated in simulation, and a first experimental investigation is discussed.**

I. Introduction

The 4.0 industry concepts are now deeply anchored in the pharmaceutical field thanks to the recent developments related to process analytical technologies (PAT). Spectroscopic probes such as Raman or fluorescent probes are more and more exploited in bioreactor monitoring setups since they can be calibrated, using chemometric models, to provide rich and useful information on culture key metabolites [1], [2]. The latter confirms the increasing success of artificial intelligence and digital tools such as dynamic models for industrial development.

The production of vaccines is usually achieved by viral amplification techniques in bioreactors, where animal host cells are first grown before being infected with a specific virus. The literature on viral amplification dynamic modeling proposes several models of different animal cell strains such as MDCK, Vero, or hybridoma [3], [4], [5], [6], [7] focusing on Influenza, Polio or Dengue. These mechanistic models have good predictive capabilities and offer the possibility to develop advanced online monitoring tools such as software sensors [8], [9], which help design the bioprocess digital twin. The application of mechanistic-model-based soft sensors to animal cell cultures, using the Extended Kalman Filter (EKF), has shown promising performance [10]. Indeed, in a recent study [11], a first soft sensor design has successfully been achieved for monitoring viral amplification on Vero cell cultures, accurately estimating virus titers that are not measurable online. The current work aims to exploit this soft sensor by proposing an optimizing control framework for budding viral amplification cultures.

[1]Laurent Dewasme, and Alain Vande Wouwer are with Systems, Estimation, Control and Optimization Group, University of Mons, 7000 Mons, Belgium <laurent.dewasme, alain.vandewouwer>@umons.ac.be

[2] Guillaume Jeanne and Lydia Saint Cristau are with Manufacturing Sciences, Analytics and Technology (MSAT) department, Sanofi, Marcy l'Etoile, France

Quality-by-design approaches ensure the quality of an industrial final product under strict constraints. The deriving good manufacturing practice (GMP) conditions apply to key species such as model state variables. Model predictive control (MPC) is well-adapted to such constrained optimization problems [12], [13]. While classical industrial applications often require tracking specific variable trajectories (i.e., regulating metabolite concentrations in the present case), economic criteria such as process production or productivity, energy consumption, or consumable savings may also be required [14]. The proposed MPC strategy should regulate the main substrate to favor the growth conditions while optimizing the infection titer quantity.

This study, included in a vaccine development project framework, reports on the control setup and its early experimental investigations.

The rest of the paper is organized as follows. Section II presents the process, the dynamic model, and a summary of the soft sensing design. The soft-sensor-based MPC problem is developed and commented on in section III, while early simulation and experimental results are discussed in section IV. Conclusions are drawn in section V.

II. Viral amplification process

A. Plant description

The budding viral amplification process is achieved in 12 L bioreactors, starting with cell seeding at day 0 followed by a fed-batch culture. At day 3, the cells are infected with the virus at a concentration calculated by a specific multiplicity of infection representing the ratio $MOI = \frac{Vir}{X}$ (which is not divulged for the sake of confidentiality). Vir and X respectively stand for the viral (Vir, 10^6 $virus/mL$) and cell (biomass X, 10^6 $cells/mL$) concentrations. Online measurements of the biomass, two substrates (S_1 and S_2, g/L), and a by-product (P_1, g/L), are taken every 20 minutes by a calibrated Raman probe. Off-line measurements also consider two other products P_2 (in mM) and P_3 (in g/L). The nature of all substrates and products must also remain undefined for confidentiality. The infection titer (IT, $log(Vir)$), which is the logarithm of the viral concentration, is not measurable online, and we resort to the EKF designed in [11] to provide an online IT (or Vir) estimate.

To illustrate the process principle, the time evolutions of the variables are shown in Figure 1, taken from the classical operation described in [11]. Biomass densification is achieved in a first batch phase followed, after three days, by the infection step combined with a medium change. Instead of

regulating the substrate concentrations, substrate depletion is avoided by repeated medium changes scheduled during the post-infection phase. These operating conditions remain manually controlled, resulting in an uncertain process yield. In the following, a model predictive controller is proposed to regulate the first substrate S_1 concentration online in a fed-batch phase, replacing several medium change steps while maximizing viral amplification.

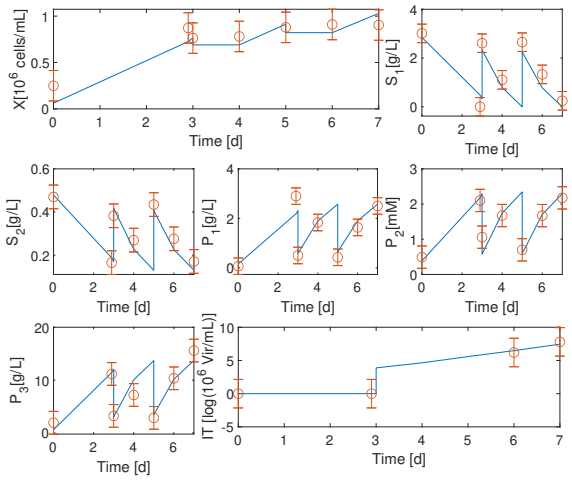

Fig. 1: Classical operation of the viral amplification process using several medium change steps defining a series of batch cultures. Continuous line: model prediction from [11]. Bubbles: experimental data with 95 % confidence intervals.

B. Dynamic model

We briefly present the main assumptions of the modeling procedure reported in [7]:

- The biomass drives the metabolite (i.e., substrates and products) dynamics;
- Only the uninfected biomass manages to divide and grow;
- Viral amplification is carried by the infected biomass;
- The infected biomass is assumed to be in a quasi-steady state compared to other slower state dynamics, resulting from a fast-slow dynamics assumption (the conversion of uninfected to infected biomass is assumed to be instantaneous).

The proposed dynamic model is described by the following generic ordinary differential equation system :

$$\frac{d\xi}{dt} = K\ \varphi \tag{1}$$

where ξ is the state vector, containing all key-species concentrations, i.e., biomass X, substrates S_1, S_2, S_3, products P_1, P_2, P_3 and the viral concentration Vir. K is the yield matrix which reads:

$$K = \begin{pmatrix} 1 & 0 & 0 \\ 0 & -Y_{S_1} & 0 \\ 0 & -Y_{S_2} & 0 \\ 0 & Y_{P_1} & 0 \\ 0 & Y_{P_2} & 0 \\ 0 & Y_{P_3} & 0 \\ 0 & 0 & Y_{Vir} \end{pmatrix} \tag{2}$$

where $Y(.)$ are the stoichiometric coefficients and the reaction rate vector φ reads:

$$\varphi = \begin{pmatrix} \mu_{growth}(X - X_i) \\ \mu_{growth} X \\ X_i \end{pmatrix} \tag{3}$$

where:

$$\mu_{growth} = \frac{-1}{1 + exp\,(-S\,(X - X_{max}))} + 1 \tag{4}$$

S characterizes the surface of the carrier beads, assumed to be known and set to 4 in the current study, and X_{max} is the maximum capacity concentration of biomass clustered on the beads. This growth rate proposed in [11] describes the biomass growth as a logistic phenomenon since perfect feeding conditions are assumed (see the multiple medium renewals in [11]) such that no substrate is ever exhausted. In most fed-batch process operating conditions, the growth rate is also driven by substrate activation factors generally modeled with Monod kinetics [15], and possible growth inhibition factors [16] following the accumulation of inhibitory by-products. Three additional factors have, therefore, been added to the growth rate to account for possible substrate limitation and growth inhibition by product accumulation in the plant. The resulting growth rate of the plant model reads:

$$\mu_{growth,plant} = \mu_{growth} \frac{S_1}{S_1 + K_{S_1}} \frac{S_2}{S_2 + K_{S_2}} \frac{K_{i,P_1}}{K_{i,P_1} + P_1} \tag{5}$$

where K_{S_1} and K_{S_2} are the half-saturation constants of the corresponding Monod factors and K_{i,P_1} is the product inhibition constant.

The infected biomass X_i is calculated as:

$$X_i = \frac{Vir}{Vir + K_{Vir}} X \tag{6}$$

where K_{Vir} stands as the half-saturation constant of the infection rate, also structured as a Monod law. Equation (6) is obtained considering a fast-slow dynamic assumption of the infection, which is assumed to be much faster than the biomass growth (see [7]).

The fed-batch conditions require to include the inlet feed flow rate in (1), which becomes:

$$\frac{d\xi}{dt} = K\ \varphi + D(\xi_{in} - \xi) = f(\xi(t), u(t)) \tag{7}$$

where $D = \frac{F_{in}}{V} = u$ is the dilution rate (the ratio of the feed flow rate F_{in} over the bioreactor volume V with dynamics $\dot{V} = F_{in}$), sole input of the process. ξ_{in} is the inlet feed concentration

vector. Since the feed medium is assumed to only contain S_1, it can be written $\xi_{in} = [0\ S_{1,in}\ 0\ 0\ 0\ 0\ 0]$.

All parameter values from [11] are reported in Table I.

TABLE I: Parameter values of model (7)

Parameter	Value	Unit
X_{max}	0.84	$10^6 cells/mL$
Y_{S_1}	3.56	$(gS_1/L)/(10^6 cells/mL)$
Y_{S_2}	0.44	$(gS_2/L)/(10^6 cells/mL)$
Y_{P_1}	3.05	$(gP_1/L)/(10^6 cells/mL)$
Y_{P_2}	2.7	$mMP_2/(10^6 cells/mL)$
Y_{P_3}	16.3	$(gP_3/L)/(10^6 cells/mL)$
Y_{Vir}	305	$10^6 virus/10^6 cells$
K_{Vir}	125	$10^6 virus/mL$
K_{S_1}	0.5	g/L
K_{S_2}	0.1	g/L
K_{i,P_1}	3	g/L

C. Infection titer estimation by Kalman Filtering

The online measurements of biomass, substrates, and product P_1 are delivered by a chemometric model (which, for the sake of confidentiality, is not presented in this paper) receiving Raman probe spectrum information at a specific sampling period T_S. From the observability analysis led in [11], the infection titer was shown to be accurately estimable, while P_2 and P_3 concentration estimates would not converge toward their actual trajectories. However, under the assumption of a small initial error on the corresponding estimates, no larger divergence of P_2 and P_3 is expected (see [11] for more details).

The EKF is a popular approach for process monitoring due to its capacity to take measurement noise into account (under the assumption of Gaussian white noises), and its successful application in many reported studies [17], [10], [18]. Due to the continuous form of (7) and the discrete-time measurements of the Raman probe, a continuous-discrete EKF form is adopted in the following, conformably to [11] where all equations of the prediction and correction steps are described. The reader may refer to this work for further details.

III. Model predictive controller design

As previously stated, the viral amplification process is divided into two phases: cell growth and infection. During the first phase, the objective is to maintain the main substrate concentration S_1 at a sufficient level to reach a dense biomass. This constitutes the following nonlinear programming problem, to be solved over a specific moving prediction horizon of size H_p:

$$\min_{u(t)} \sum_{t=t_i}^{t_i+H_p-1} (S_1(t) - S_{1,ref})^2 \tag{8a}$$

$$s.t. \quad \dot{\xi} = f(\xi(t), u(t)) \tag{8b}$$

$$u(t) = u(t_i + H_c - 1), \quad t \in [t_i + H_c, t_i + H_p - 1] \tag{8c}$$

$$u_L \leq u(t) \leq u_U, \quad t \in [t_i, t_i + H_p - 1] \tag{8d}$$

$$\Delta u_L \leq \Delta u(t) \leq \Delta u_U, \quad t \in [t_i, t_i + H_p - 1] \tag{8e}$$

$$\xi_L \leq \xi(t) \leq \xi_U, \quad t \in [t_i, t_i + H_p - 1] \tag{8f}$$

the index i spans the prediction horizon (i.e., starting at sample k and finishing at sample $k+H_p-1$) and u is the input vector of dimension H_c representing the control horizon.

L and U lower indices denote lower and upper bounds of the control u, the control variation Δu and the states ξ. u_L was set to 0 and u_U to 1 $L\ d^{-1}$ while $\Delta u_L = \Delta u_U = 0.1\ L\ d^{-1}$. State bounds were defined such that all state values simply remain positive ($\xi_L = 0$, and $\xi_U = +\infty$).

The second phase is dedicated to the maximization of the virus titer. The corresponding optimization problem is formulated as follows:

$$\min_{u(t)} \sum_{t=t_i}^{t_i+H_p-1} -Vir(t) \tag{9a}$$

$$s.t. \text{(8b) to (8f)} \tag{9b}$$

Considering both phases of cell culture and the growth rate (5) activated by the substrates, criteria (8a) and (9a) merge into the following new criterion with additional substrate penalties:

$$\min_{u(t)} \sum_{t=t_i}^{t_i+H_p-1} -Vir(t) + \gamma\ (S_1(t) - S_{1,ref})^2 \tag{10a}$$

$$s.t. \text{(8b) to (8f)} \tag{10b}$$

where $S_{1,ref}$ is the substrate reference to be maintained to activate (5), and γ is the corresponding penalty weight. It should be noted that S_2 is assumed to be initially fed in sufficient quantity and is, therefore, not fed during the fed-batch phase.

IV. MPC validation

A. Numerical results

In the following simulation results, the controller is assumed to compute the state predictions using the nominal kinetic model (3) with the growth rate defined in (4) while the actual plant model is driven by (5). The controller plus soft sensor performance is, in this way, challenged with structural model uncertainties.

Table II reports the controller parameter values and the operating conditions. The time of infection is set to day 3 with a multiplicity of infection (MOI) defined as $MOI = \frac{Vir(T_{inf})}{X(T_{inf})}$

(the value is not revealed for the sake of confidentiality) where T_{inf} is the infection time. γ was set to 10, considering the orders of magnitude of Vir and S_1.

TABLE II: Operating and control parameters of the simulated viral amplification process.

Parameter	Value
T_S	0.1 day
H_p	0.4 day
H_c	0.2 day
T_{inf}	3 $days$
$S_{1,ref}$	2 g/L
γ	10
$S_{1,in}$	450 g/L

The EKF is parameterized following the guidelines of [11]. It should be noted that the EKF model is augmented with the growth rate μ_{growth}, which can also be estimated assuming zero dynamics (i.e., the growth rate is assumed to vary slowly, and the EKF uses an "exogenous" form of the model):

$$\frac{d\mu_{growth}}{dt} = 0 \tag{11}$$

Figure 2 presents the state trajectories. All states except P_2, P_3, and Vir (or IT) are assumed to be measured online with measurement noise standard deviations reported in [11]. S_1 concentration is regulated around $S_{1,ref} = 2\ g/L$, allowing the biomass to grow at a sufficient rate (5), even though the MPC uses the nominal model (4). Figure 3 shows the corresponding feed rate trajectory.

After three days, the infection is launched, and the viral amplification phase starts. This provokes a sudden series of feeding peaks (see Figure 3) to maintain S_1 concentration from day 4 to 7. In the meantime, the infection titer (the logarithm of the viral concentration) exponentially increases. S_1 concentration remains around the desired reference value while the growth rate decreases with time due to viral amplification. These latter signals both remain well estimated despite the sudden cell metabolic changes. S_2 concentration remains around 1 g/L (the signal is corrupted by a high noise level) and is slowly consumed. The biomass saturation occurring from day 5 until 7 is mainly due to the combination of a low growth rate explained by a high P_1 concentration (almost 3 g/L), combined with the exponential infection of the remaining biomass.

B. Experimental investigations

The simulated scenario of section IV-A has been reproduced at an experimental lab scale in the Sanofi laboratories with the same controller parameters. Figure 4 illustrates the feedback control principle: an immerged Raman probe provides online measurements under the form of spectra every 0.1 day, and a calibrated chemometric model interprets these spectra to provide X, S_1, S_2 and P_1 to a data acquisition LabView platform where the predictive controller and the soft sensor are coded in a Matlab node. The LabView platform sends the computed feed flow rate value to a peristaltic pump connecting the medium tank to the bioreactor.

Figure 5 shows the trajectories of the state variables and the cell growth rate. Following some technical issues with the Raman probe, the biomass concentration was only detected after two days, and Figure 5 graphs, therefore, start one day before infection, assumed to be at $t = 1\ day$ (actually corresponding to 65 hours of culture). The controller and the soft sensor were however running and it can be observed that despite the wrong expected model state trajectories (in orange), the EKF was able to converge to the Raman signal recovered on day 1.

S_1 concentration remained well regulated and S_2 concentration, as expected from the results shown in Figure 2, was slowly consumed over the experiment period of almost 4 days. The probe failure generated some issues in estimating the other metabolites, expecting a greater accumulation of P_1 and probably of P_2 and $P3$, which were not measured. It can however be appreciated how the EKF managed to smooth the biomass, S_1, and S_2 trajectories despite the chaotic evolution of the Raman probe measurements.

The biomass growth was maintained before a plateau, as already observed in Figure 2, suggesting a probable Raman probe inaccuracy in measuring P_1 concentration. Regardless, the EKF smoothed the growth rate estimation at a consistent positive value. The estimated infection titer showed an overestimation of the virus concentration by the model, and the resulting EKF estimate from Figure 5 reaches a consistent value with the predictions from Figure 2. For the sake of confidentiality, offline measurements were voluntarily removed from these results.

Despite the probe failures, the proposed methodology, tested in simulation, was satisfactorily reproduced in experimental conditions. Moreover, the EKF showed a good adaptation to difficult measuring circumstances. The provided estimates remained consistent, and S_1 was well regulated at $S_{1,ref} = 2\ g/L$.

V. Conclusion

Combining a control strategy with a software sensor is a challenging but promising methodology with still few experimental validations in the bioprocess control literature [19], [20], [18]. To the authors' knowledge, this study is the first to propose the application of this control setup to the monitoring and control of the fed-batch viral amplification process. Based on a previous validation of the software sensor by the same authors, a nonlinear model predictive control policy, using online-delivered biomass and metabolite estimates, is proposed and validated in simulation to regulate the main substrate concentration level, guaranteeing a sufficient cell growth rate, while maximizing virus production. Both simulated and experimental results show the effectiveness of the method in regulating the main substrate concentration while maintaining the viral amplification in the fed-batch process. Further research entails (1) new validations in the same experimental environment while reinforcing the Raman probe calibration to

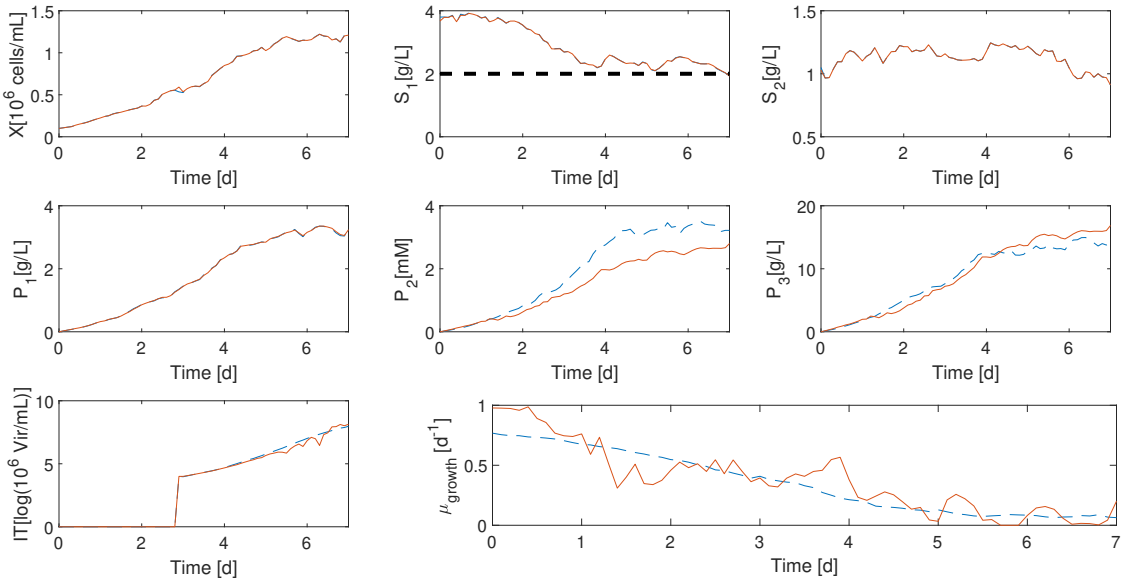

Fig. 2: Nonlinear MPC application using the nominal model (4) for prediction and (5) as actual plant kinetics. Continuous line: simulated plant trajectories. Blue dashed line: extended Kalman filter estimates. Black dashed line: $S_{1,ref}$.

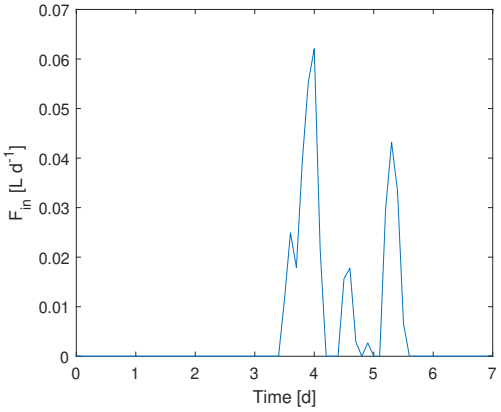

Fig. 3: NMPC application using the nominal model (4) for prediction and (5) as actual plant kinetics - Input u trajectory.

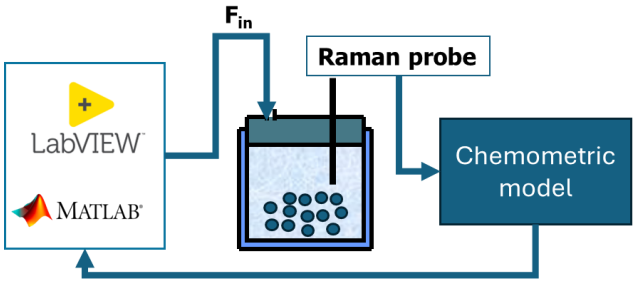

Fig. 4: Experimental setup of the fed-batch process development environment of viral amplification in Sanofi.

deliver more accurate biomass and metabolite online measurements, and (2) the implementation and validation of a robust control strategy such as tube-based or multi-stage MPC, taking into account and reducing the undesired effects of model uncertainties and measurement noise [21], [22].

Acknowledgment

This work was funded by Sanofi. Conceptualization, investigation, methodology, software, and original draft preparation: Laurent Dewasme. Resources and data curation: Lydia Saint Cristau and Guillaume Jeanne. Methodology and writing review-editing: Alain Vande Wouwer. Lydia Saint Cristau and Guillaume Jeanne are Sanofi employees and may hold shares in the company. All other authors declare no competing interests and have read and agreed to the published version of the manuscript.

References

[1] H. Bhatia, H. Mehdizadeh, D. Drapeau, and S. Yoon, "In-line monitoring of amino acids in mammalian cell cultures using raman spectroscopy and multivariate chemometrics models," *Engineering in Life Sciences*, vol. 18, no. 1, pp. 55–61, 2018.

[2] A. Yousefi-Darani, O. Paquet-Durand, A. von Wrochem, J. Classen, J. Tränkle, M. Mertens, J. Snelders, V. Chotteau, M. Mäkinen, A. Handl, M. Kadisch, D. Lang, P. Dumas, and B. Hitzmann, "Generic chemometric models for metabolite concentration prediction based on raman spectra," *Sensors*, vol. 22, no. 15, 2022.

[3] L. Möhler, D. Flockerzi, H. Sann, and U. Reichl, "Mathematical model of influenza a virus production in large-scale microcarrier culture," *Biotechnology and bioengineering*, vol. 90, no. 1, pp. 46–58, 2005.

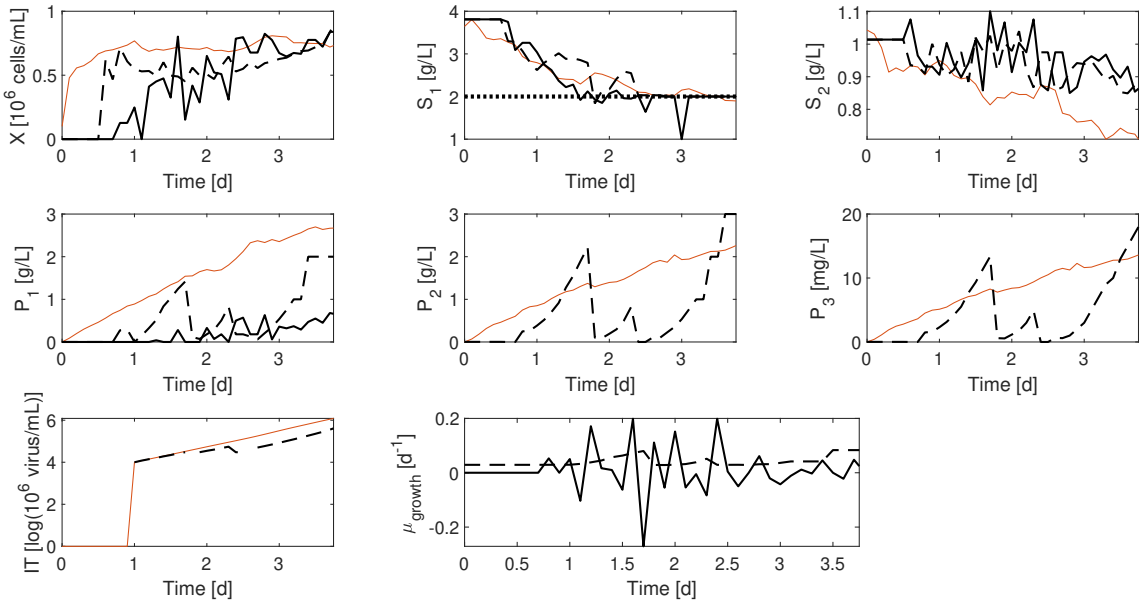

Fig. 5: Experimental validation of the NMPC during viral amplification. Continuous orange line: simulated plant trajectories. Continuous black line: Raman probe measurements. Dashed line: extended Kalman filter estimates. Dotted line: $S_{1,ref}$.

[4] J. Schulze-Horsel, M. Schulze, G. Agalaridis, Y. Genzel, and U. Reichl, "Infection dynamics and virus-induced apoptosis in cell culture-based influenza vaccine production—flow cytometry and mathematical modeling," *Vaccine*, vol. 27, no. 20, pp. 2712–2722, 2009.

[5] T. Müller, R. Dürr, B. Isken, J. Schulze-Horsel, U. Reichl, and A. Kienle, "Distributed modeling of human influenza a virus–host cell interactions during vaccine production," *Biotechnology and Bioengineering*, vol. 110, no. 8, pp. 2252–2266, 2013.

[6] R. V. Ursache, Y. E. Thomassen, G. van Eikenhorst, P. J. Verheijen, and W. A. Bakker, "Mathematical model of adherent vero cell growth and poliovirus production in animal component free medium," *Bioprocess and biosystems engineering*, vol. 38, pp. 543–555, 2015.

[7] T. Abbate, L. Dewasme, and A. Vande Wouwer, "Variable selection and parameter estimation of viral amplification in vero cell cultures dedicated to the production of a dengue vaccine," *Biotechnology Progress*, vol. 35, no. 1, p. e2687, 2019.

[8] D. Dochain, "State and parameter estimation in chemical and biochemical processes: a tutorial," *Journal of Process Control*, vol. 13, no. 8, pp. 801–818, December 2003.

[9] P. Bogaerts and A. Vande Wouwer, "Software sensors for bioprocesses," *ISA Transactions*, vol. 42, pp. 547–558, 2003.

[10] L. Dewasme, S. Fernandes, Z. Amribt, L. Santos, P. Bogaerts, and A. Vande Wouwer, "State estimation and predictive control of fed-batch cultures of hybridoma cells," *Journal of Process Control*, vol. 30, pp. 50–57, 2015.

[11] L. Dewasme, G. Jeanne, L. Saint Cristau, C. Barraud, and A. V. Wouwer, "Advanced monitoring of viral amplification process by soft sensing," *IFAC-PapersOnLine*, vol. 55, no. 20, pp. 487–492, 2022.

[12] S. J. Qin and T. A. Badgwell, "A survey of industrial model predictive control technology," *Control Engineering Practice*, vol. 11, pp. 733 – 764, 2003.

[13] E. Bolmanis, K. Dubencovs, A. Suleiko, and J. Vanags, "Model predictive control—a stand out among competitors for fed-batch fermentation improvement," *Fermentation*, vol. 9, no. 3, 2023.

[14] D. Angeli, R. Amrit, and J. B. Rawlings, "On average performance and stability of economic model predictive control," *IEEE Transactions on Automatic Control*, vol. 57, no. 7, pp. 1615–1626, 2012.

[15] J. Monod, "The growth of bacterial cultures," *Annual Review of Microbiology*, vol. 3, no. 1, pp. 371–394, 1949.

[16] N. Jerusalimski and N. Engamberdiev, *Continuous cultivation of microorganisms*. Academic Press, New York, 1969, vol. 517.

[17] L. Dewasme, G. Goffaux, A.-L. Hantson, and A. Vande Wouwer, "Experimental validation of an extended kalman filter estimating acetate concentration in *E. coli* cultures," *Journal of Process Control*, vol. 23, pp. 148–157, 2013.

[18] M. Abadli, L. Dewasme, S. Tebbani, D. Dumur, and A. Vande Wouwer, "Experimental validation of a nonlinear model predictive controller regulating the acetate concentration in fed-batch escherichia coli bl21 (de3) cultures," *Advanced Control for Applications: Engineering and Industrial Systems*, vol. 4, no. 1, p. e95, 2022.

[19] L. Dewasme, A. Richelle, P. Dehottay, P. Georges, M. Remy, P. Bogaerts, and A. Vande Wouwer, "Linear robust control of *S. cerevisiae* fed-batch cultures at different scales," *Biochemical Engineering Journal*, vol. 53, no. 1, pp. 26–37, December 2010.

[20] M. Abadli, L. Dewasme, S. Tebbani, D. Dumur, and A. Vande Wouwer, "An experimental assessment of robust control and estimation of acetate concentration in escherichia coli bl21(de3) fed-batch cultures," *Biochemical Engineering Journal*, vol. 174, p. 108103, 2021.

[21] L. Dewasme, M. Mäkinen, and V. Chotteau, "Practical data-driven modeling and robust predictive control of mammalian cell fed-batch process," *Computers and Chemical Engineering*, vol. 171, p. 108164, 2023.

[22] ——, "Multivariable robust tube-based nonlinear model predictive control of mammalian cell cultures," *Computers & Chemical Engineering*, vol. 183, p. 108592, 2024.